Satellite and Aircraft Observations of the Eyewall Replacement Cycle in Typhoon Sinlaku (2008)

ELIZABETH R. SANABIA AND BRADFORD S. BARRETT

Oceanography Department, U.S. Naval Academy, Annapolis, Maryland

NICHOLAS P. CELONE

Helicopter Sea Combat Squadron Two Three (HSC-23), U.S. Navy, San Diego, California

ZACHARY D. CORNELIUS

Training Squadron Three (VT-3), U.S. Navy, Milton, Florida

(Manuscript received 17 February 2015, in final form 22 May 2015)

ABSTRACT

Satellite and aircraft observations of the concurrent evolution of cloud-top brightness temperatures (BTs) and the surface and flight-level wind fields were examined before and during an eyewall replacement cycle (ERC) in Typhoon Sinlaku (2008) as part of The Observing System Research and Predictability Experiment (THORPEX) Pacific Asian Regional Campaign (T-PARC) and the Tropical Cyclone Structure 2008 (TCS08) field campaign. The structural evolution of deep convection through the life cycle of the ERC was clearly evident in the radial variation of positive water vapor (WV) minus infrared (IR) brightness temperature differences over the 96-h period. Within this framework, the ERC was divided into six broadly defined stages, wherein convective processes (including eyewall development and decay) were analyzed and then validated using microwave data. Dual maxima in aircraft wind speeds and geostationary satellite BTs along flight transects through Sinlaku were used to document the temporal evolution of the ERC within the TC inner core. Negative correlations were found between IR BTs and surface wind speeds, indicating that colder cloud tops were associated with stronger surface winds. Spatial lags indicated that the strongest surface winds were located radially inward of both the flight-level winds and coldest cloud tops. Finally, timing of the ERC was observed equally in IR and WV minus IR (WVIR) BTs with one exception. Decay of the inner eyewall was detected earlier in the WVIR data. These findings highlight the potential utility of WVIR and IR BT radial profiles, particularly so for basins without active aircraft weather reconnaissance programs such as the western North Pacific.

1. Introduction

Accurate analyses of the structure of the surface wind field in a tropical cyclone (TC) are critical to enhancing readiness and mitigating risk for coastal populations. In landfalling systems, the radial locations of critical wind speeds guide disaster preparation and provide proper vortex initialization in numerical models. However, determining the inner core and surface wind field structure of TCs remains a considerable operational challenge to the TC community. For example, in the western North Pacific Ocean, initial estimation of radii of 34-, 50-, and 64-kt winds ($1\,\text{kt} = 0.51\,\text{m s}^{-1}$) by forecasters at the Joint Typhoon Warning Center (JTWC) remains rather subjective and strongly dependent on sparsely available observations (Kossin et al. 2007; Knaff et al. 2007). Furthermore, while many theoretical models have been developed to simulate the radial distribution of surface winds in a TC (Holland 1980; DeMaria 1987; Leslie and Holland 1995; Emanuel 2004; Emanuel et al. 2006; Willoughby et al. 2006; Holland et al. 2010; Knaff et al. 2011; Wood et al. 2013), a great deal of variability has been observed in TC wind field size (Lee et al. 2010). One of the reasons for this variability is that surface winds in a TC are strongly controlled by dynamical processes known to affect inner-core structure. The

Corresponding author address: Elizabeth R. Sanabia, 572C Holloway Rd., Annapolis, MD 21402.
E-mail: sanabia@usna.edu

DOI: 10.1175/MWR-D-15-0066.1

formation of concentric eyewalls (CEs) and the progression of deep convection through an eyewall replacement cycle (ERC) are two examples of dynamical processes that have been shown to exert significant control on TC surface wind field structure (Willoughby et al. 1982; Black and Willoughby 1992; Kuo et al. 2009; Sitkowski et al. 2011; Wood et al. 2013). Secondary eyewall formation and ERCs were also found to be responsible for significant changes in area-integrated kinetic energy of the TC (Maclay et al. 2008). Concentric eyewalls have been found in upward of 80% of western North Pacific typhoons with maximum surface winds above 120 kt (Hawkins and Helveston 2004), indicating that they are a common feature of strong typhoons. Furthermore, because surface wind speed often weakens while the wind field expands during the ERC process, CEs often complicate the operational TC forecast (Kossin and Sitkowski 2009). Despite their frequency, in basins without routine aircraft reconnaissance, such as the western North Pacific Ocean, the primary data source used to operationally identify CE structures is infrequently and irregularly available microwave satellite observations (Kuo et al. 2009; Yang et al. 2013). Thus, techniques that can identify possible CEs and map their changes as part of ERCs using regularly available observations, including those from geostationary satellites, would be potentially useful in an operational setting.

Strong TCs often have been observed with an inner (primary) and outer (secondary) eyewall separated by a region of minimal convection (Willoughby et al. 1982). Although variable and not always completed, the ERC typically begins with the formation of the outer eyewall, continues as convection intensifies in the outer eyewall and weakens in the inner eyewall, and concludes as the inner eyewall fully decays and the outer eyewall contracts toward the storm center (Rozoff et al. 2008; Sitkowski et al. 2011; Kossin and Sitkowski 2012; Abarca and Montgomery 2013). Important intensity changes occur concurrently with these changes in convective structure, so much so that Sitkowski et al. (2011) classified ERCs into three intensity-based phases: intensification, weakening, and reintensification. As the outer eyewall forms and inner eyewall decays, the TC often weakens and the surface wind field broadens (Sitkowski et al. 2011; Kepert 2013); once the surface wind speed at the outer eyewall surpasses the surface wind speed at the inner eyewall, the storm may begin to intensify as the inner eyewall dissipates (Sitkowski et al. 2011).

In recent modeling studies, ERCs were found to take between 6 and 18 h to complete (Terwey and Montgomery 2008; Zhou and Wang 2009; Qiu et al. 2010). In an observational study based on Atlantic and central and eastern Pacific basin aircraft reconnaissance data, the ERC process was found to be slower, taking upward of 36 h to complete, although considerable storm-to-storm variability was noted (Sitkowski et al. 2011). Despite these findings, CE structure and ERC processes remain challenging to observe in real time. Hurricane Rita was a rare case in which detailed finescale convective and wind structures were extensively observed throughout an ERC. Aircraft and dual Doppler radar observations (Houze et al. 2006, 2007; Bell et al. 2012) captured the temporal and spatial behavior both eyewalls during Rita and provided the opportunity for in-depth analysis. One of the objectives of the current study is to present a geostationary satellite-based technique that highlights the structural evolution of deep convection during the ERC of Typhoon Sinlaku (2008). Given the role of boundary layer dynamics in ERCs [e.g., the boundary layer spinup mechanisms proposed by Abarca and Montgomery (2014, 2015)], another objective is to compare the evolution of deep convection with the concurrent evolution of the surface and flight-level wind measurements within and above the boundary layer, respectively. The surface winds were measured by the Stepped-Frequency Microwave Radiometer (SFMR), and the flight-level winds were computed by the aircraft data system, both on board the WC-130J. By analyzing this western North Pacific ERC within a framework based on deep convection, it is hoped that the results may be useful to warning centers in regions without active aircraft weather reconnaissance programs. The remainder of the paper is organized as follows: a brief synoptic summary of Sinlaku is presented in section 2, data and methodology are presented in section 3, results are presented in section 4, and conclusions are presented in section 5.

2. Typhoon Sinlaku (2008) synoptic overview

Typhoon Sinlaku (2008) was extensively observed during two collaborative experiments, The Observing System Research and Predictability Experiment (THORPEX) Pacific Asian Regional Campaign (T-PARC; Elsberry and Harr 2008; Chou et al. 2011; Weissmann et al. 2011) and Tropical Cyclone Structure 2008 (TCS08; Elsberry and Harr 2008). Sinlaku formed east of the Philippines and was named by the Joint Typhoon Warning Center at 0000 UTC 9 September 2008. Over the next 36 h, the system intensified from winds of 35 kt to winds of 100 kt (Cooper et al. 2009), exceeding the definition of rapid intensification set forth by Kaplan and DeMaria (2003), and reached its maximum intensity (125 kt) at 1800 UTC 10 September 2008 (Fig. 1). From

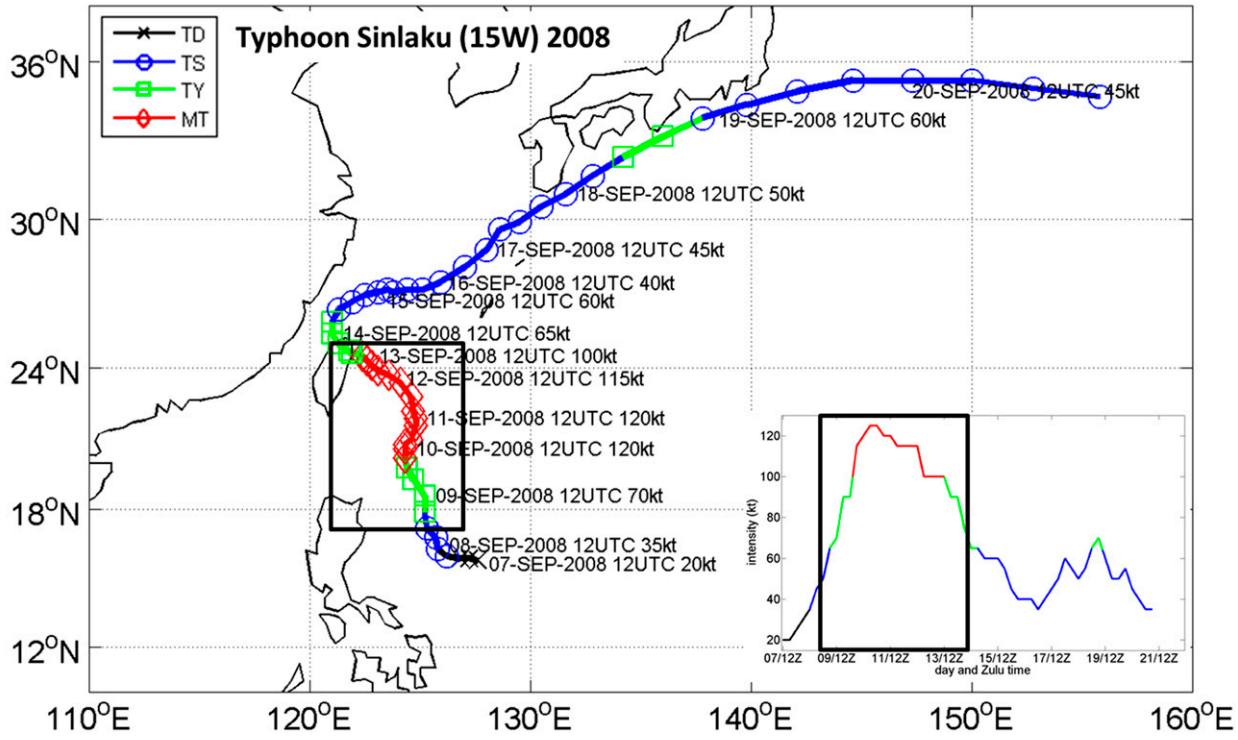

FIG. 1. Track and intensity of Typhoon Sinlaku (2008). Surface winds less than 34 kt indicated by black crosses, 34– 63 kt by blue circles, between 64–99 kt by green squares, and ≥100 kt by red diamonds. Black boxes indicate the region of emphasis for this study.

10 to 12 September 2008, Sinlaku underwent an eyewall replacement cycle. On 11 September 2008, a clear CE structure was noted on microwave satellite imagery from 0445 to 2132 UTC, and this structure was confirmed during a reconnaissance mission within that period that found dual wind maxima on both inbound and outbound legs during transects with center fix times of 1207 and 1331 UTC 11 September 2008 (Middlebrooke and Sanger 2008). Sinlaku made landfall near Taipei, Taiwan, on 13 September 2008 (Cooper et al. 2009), then recurved, and subsequently weakened to an intensity of 35 kt at 0000 UTC 17 September 2008 before intensifying again on approach to Japan. This study is focused on the 5-day period from classification as a tropical storm in the Philippine Sea to landfall over Taiwan (black boxes, Fig. 1).

3. Data and methodology

a. Data

Satellite and aircraft-based observations of Typhoon Sinlaku formed the basis for this study. In both datasets, critical emphasis was given to the ERC time frame (10–13 September 2008). Satellite imagery was provided by the Naval Research Laboratory–Monterey from both geostationary (for infrared and water vapor imagery) and polar-orbiting (for microwave imagery) platforms. Satellite brightness temperature (BT) digital data were used to quantitatively assess deep convection during the ERC. Water vapor (WV; 6.7 μm) and infrared (IR; 10.6 μm) BTs from the geostationary *Multifunctional Transport Satellite-1* (*MTSAT-1*) were provided by the Japan Meteorological Agency (JMA). These 4-km data were collected at 30-min intervals (with occasional brief lapses for maintenance) as part of the T-PARC and TCS08 field programs. During the 120-h period of this study, there were 200 geostationary (WV and IR) satellite datasets. Aircraft data were collected during four WC-130J flights by the U.S. Air Force (USAF) 53rd Weather Reconnaissance Squadron (53rd WRS). Surface and flight-level wind speeds and directions, recorded by the SFMR and aircraft data system, respectively, were combined with the WC-130J GPS position every 30 s in High Density Observation (HDOB) messages. The TC track and intensity data included in this study were taken from the JTWC Best Track archive (available in text format online at http://www.usno.navy.mil/NOOC/nmfc-ph/RSS/jtwc/best_tracks/2008/2008s-bwp/bwp152008.txt).

TABLE 1. List of WC-130J center transects through Typhoon Sinlaku and corresponding *MTSAT-1* satellite observation times during the period of this study.

Center transect	Date	First aircraft observation		Final aircraft observation		Satellite observation
		Time (UTC)	Position (relative to TC center)	Time (UTC)	Position (relative to TC center)	Time (UTC)
1	9 Sep 2008	0420	South	0526	North	0445
2	9 Sep 2008	0600	West	0710	East	0645
3	10 Sep 2008	0540	Southeast	0642	Northwest	0545
4	10 Sep 2008	0715	Southwest	0826	Northeast	0745
5	11 Sep 2008	1135	Southeast	1234	Northwest	1145
6	11 Sep 2008	1305	Southwest	1406	Northeast	1345
7	12 Sep 2008	1627	Southeast	1725	Northwest	1645
8	12 Sep 2008	1747	Southwest	1848	Northeast	1745

b. Methodology

1) RADIAL PROFILES OF DEEP CONVECTION

In the first two parts of this study, radial profiles of satellite BTs were constructed to examine deep convection near the TC inner core. Each radial profile was examined individually, and then all were examined collectively in a Hovmöller diagram, to form an overall understanding of the evolution of deep convection through the ERC. Geostationary satellite platforms have an advantage in temporal coverage, with regular scans about every half hour (instead of every half day for polar-orbiting satellite-based sensors). However, the broad weighting function in both the IR and WV wavelengths makes it difficult to detect and isolate cores of deep convection from surrounding cloudy regions. Used together, however, the BT difference between WV and IR wavelengths utilizes the temperature inversion at the tropopause to isolate deep convection (Fritz and Laszlo 1993; Olander and Velden 2009). For this study, BT differences for each satellite time were found by subtracting IR BTs from WV BTs. Positive values indicated deep convection that had penetrated the tropopause, and deep convection identified in this manner has been found to be related to rapid intensification (Monette et al. 2012) and TC rotational intensity (Chao et al. 2011; Jaiswal et al. 2012).

To construct radial profiles, the 200 sets of IR and WV satellite observations were transformed from Cartesian to a storm-centered polar grid. While some automated center-identification techniques exist (e.g., Wimmers and Velden 2010), identifying the TC center objectively from IR and WV data still remains a challenge. Linear interpolation of the JTWC best track latitude and longitude coordinates provided the starting point for the manual identification of the TC centers. For each observation, mean positive WV minus IR (WVIR) BT difference radial profiles were created by subtracting IR BTs from WV BTs in the storm-centered coordinate system and then azimuthally averaging the positive BT differences at 1.0° theta (azimuthal spacing) intervals around the TC center at radial increments of 0.02° (about 2 km) outward from the center, following the methodology of Sanabia et al. (2014). This technique was applied to each of the 200 WVIR datasets during the 120-h period of study, and a time–radius Hovmöller diagram of the positive WVIR BT differences was created to map the radial variation in deep convection over time. Radial profiles of IR BT, which mapped radial variation in cloud-top temperature (a relative measure of cloud-top height) over time, were created in a similar way, except only IR BT values were azimuthally averaged instead of positive WVIR BT differences.

2) AIRCRAFT WIND AND SATELLITE BT COMPARISON DURING EYEWALL TRANSECTS

In the third part of the study, surface and flight-level wind speeds measured from the aircraft during transects through the TC were analyzed and compared to the convective structures identified in the satellite data. The WC-130Js made eight passes through the center of Typhoon Sinlaku during four flights between 9 and 12 September 2008 (Table 1). The passes differed in length and heading and were dependent on the flight track. During the 9 September 2008 flight, there were two passes through the Sinlaku center, a south–north pass followed by a west–east pass through the developing tropical storm. From 10 to 12 September 2008, alpha patterns were flown, with transects oriented southeast to northwest followed by southwest to northeast. The passes varied in length, but typically extended at least 120 km from the TC center. Most flight tracks were relatively straight cross sections through the TC center; however, in the final pass (second transect on 12 September 2008), several loops were flown in the eye. Data from these loops were not used in this study.

Each of the eight aircraft passes was matched in time with the closest *MTSAT-1* satellite observation (Table 1). Since each aircraft transect took approximately 1 h, the time that the center was marked in the flight-level winds (i.e., the minimum flight-level wind in the eye of the TC) was assigned to represent the transect. There were up to 30-min differences in the times representing the transects and the times of the *MTSAT-1* satellite observations (assigned by JMA). To accommodate this difference, the aircraft transects were adjusted spatially to place the aircraft center in the center of the satellite observation. Satellite IR BTs were then interpolated to the surface wind observation locations using a spline interpolation. This process was repeated for the WV BT data.

After these adjustments, the aircraft surface and flight-level wind speeds, positive WVIR BT differences and IR BT data were plotted as radial cross sections based on distance from the TC center. These radial cross sections were analyzed to identify potential relationships between the deep convection and surface and midlevel wind fields before and during the ERC. To quantify these relationships, Pearson product-moment correlations were calculated from the satellite and aircraft data along each transect within 100 km of the TC center. Spatial lags were also calculated to determine if surface and flight-level winds led or lagged the IR BT in radial distance from the TC center. For the satellite observations corresponding to each of the eight center transects, mean radial profiles of both IR BTs and positive WVIR BT differences were constructed in the manner discussed in the previous section. These mean profiles were used as a qualitative check of the representativeness of each transect and also to further investigate the temporal signal of the onset and completion of the ERC in both the IR and WVIR BTs.

4. Results

Results of the Sinlaku ERC satellite and aircraft data analysis are presented here in three sections. First, stages of the ERC are defined in terms of deep convection, and the evolution of Sinlaku through RI and those ERC stages is evaluated using WVIR BTs. Second, satellite observations of deep convection and cloud-top brightness temperatures are analyzed during the eight WC-130J passes through the TC center during the RI and ERC. Finally, relationships between deep convection, cloud-top BTs, and surface and flight-level wind speeds are analyzed along the eight aircraft transects through the TC center.

a. Evolution of deep convection during rapid intensification and ERC

For this study, the ERC of Typhoon Sinlaku was divided into six broadly defined stages, which were each defined using microwave and geostationary satellite observations. The stages and their starting and ending points are somewhat subjective but serve to emphasize convective processes as observed by satellite during the ERC. At each ERC stage, the patterns of deep convection are discussed here in terms of the radial profiles of azimuthally averaged positive WVIR BT differences. The stages presented below agree well with other ERC conceptual models (e.g., Houze et al. 2007; Sitkowski et al. 2011) and are used to classify and highlight the evolution of Sinlaku's convective structure. The convective stages of the ERC were observed were as follows:

1) Single eyewall stage. A broad, single eyewall characterized the first stage of the ERC process (row 1 in Fig. 2). In Sinlaku, the eyewall was identifiable in infrared and water vapor imagery at 1515 UTC 10 September 2008 as a broad ring of overshooting tops surrounding the eye of the storm. A second convective region was present approximately 300 km from the TC center; however, bands in this region were asymmetric.
2) Transition to concentric eyewall (CE) stage. The second ERC stage in the Sinlaku case (row 2 in Fig. 2) was marked by weakening of the inner-core convection, which was particularly evident north of the TC center at 2115 UTC 10 September 2008 (column 4). This decay in inner-core deep convection was also clear in the azimuthally averaged positive BT differences from the same time step (column 5), where lower BT differences were present beyond about 80 km from the TC center. In the 89-GHz microwave imagery between stages 1 and 2 (column 3), a convective ring within 75 km of the TC center was evident and the development of an outer convective ring was also apparent southeast and southwest of the TC center.
3) Concentric eyewall stage. The third stage of the Sinlaku ERC was characterized by a double eyewall structure (row 3 in Fig. 2). During this stage, a small inner eyewall approximately 40 km from the TC center and another broader outer eyewall extending from a radius of 120 to 200 km were clearly identifiable in the positive WVIR BT differences at 1115 UTC 11 September 2008 (column 5), along with microwave (91 GHz) imagery at 0900 UTC 11 September 2008 (column 3). This structure was replicated in numerical simulations of Sinlaku, with the development of a secondary wind maximum between 75 and 125 km from the center by 0600 UTC 11 September 2008 (Wu et al. 2012; Huang et al. 2012).

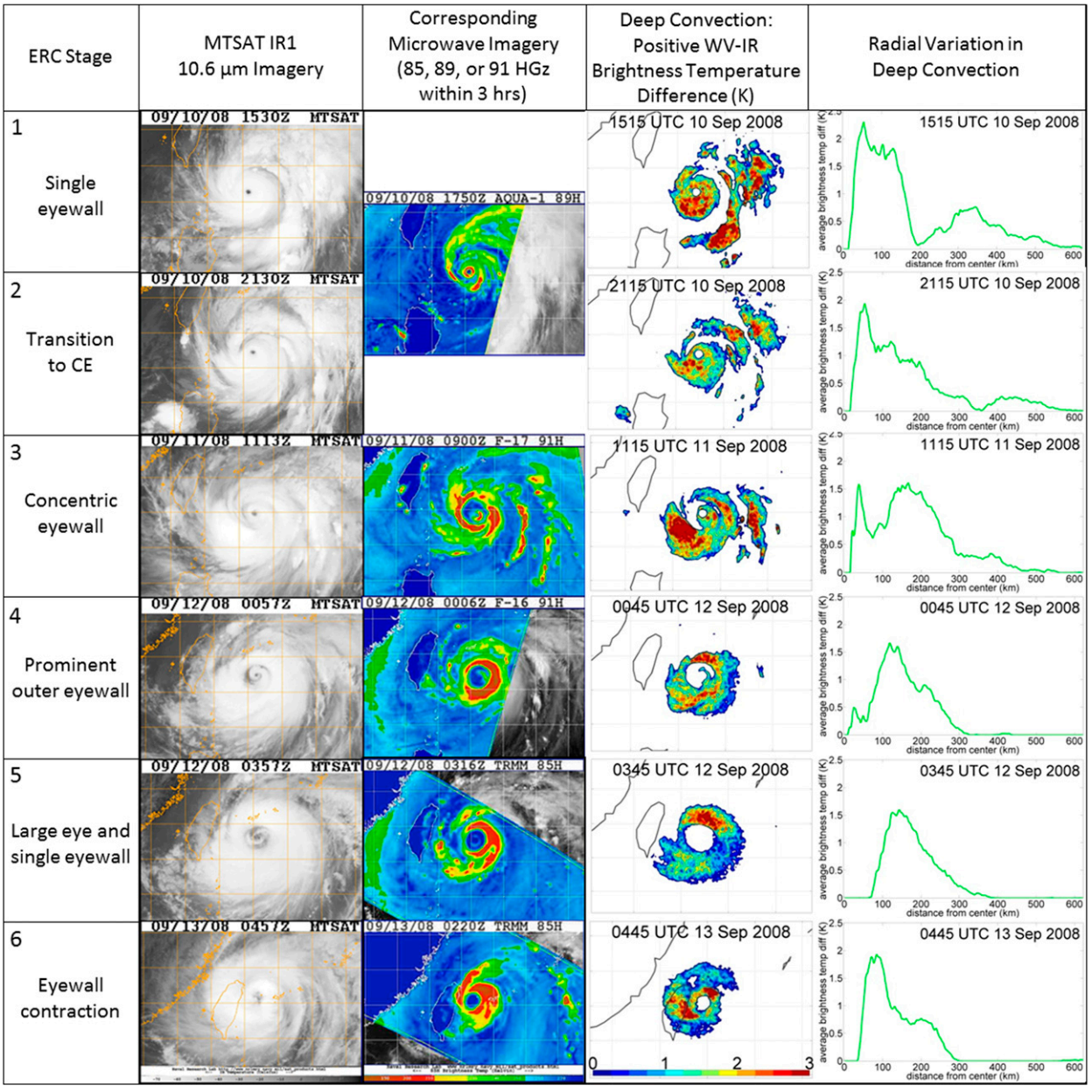

FIG. 2. (left to right) Eyewall replacement cycle (ERC) stages, IR satellite imagery, microwave satellite imagery, positive WVIR BT differences (K), and radial profiles of azimuthally averaged WVIR BT differences (K) for (from top to bottom) stages 1–6. Satellite imagery (columns 2 and 3) available online from the Naval Research Laboratory–Monterey at http://www.nrlmry.navy.mil/TC.html.

4) Prominent outer eyewall stage. The fourth stage of the Sinlaku ERC was highlighted by the decay of the inner eyewall, which was nearly complete in the early hours of 12 September 2008 (row 4 in Fig. 2). At 0045 UTC 12 September 2008 (in the WVIR BT differences, columns 4 and 5) and 0006 UTC 12 September 2008 (in the 91-GHz microwave, column 3), a single outer eyewall was centered nearly 120 km from the storm center, and weak, asymmetric, remnant convection remained within the old inner eyewall.
5) Large eye and single eyewall stage. During the fifth ERC stage (row 5 in Fig. 2), the eye was free of deep convection, with zero positive WVIR BTs at 0345 UTC 12 September 2008 from the storm center out to a radius of nearly 80 km. The single remaining eyewall was centered around 120 km from the center in both WVIR and microwave (85 GHz) imagery.

This fifth stage began once the deep convection in the inner eyewall dissipated entirely.

6) Eyewall contraction stage. The broad, outer eyewall then contracted in the sixth ERC stage (row 6 in Fig. 2). This narrowing of the eye diameter was evident in the 0445 UTC 13 September 2008 positive WVIR BT differences (columns 4–5) and the 0220 UTC 13 September 2008 85-GHz microwave imagery (column 3). It was at this point that the TC reverted back to the single eyewall profile generally consistent with the first stage of the ERC (Houze et al. 2007; Laing and Evans 2010). This progression through the ERC cycle was also simulated by Wu et al. (2012), who noted the ERC had completed by 1800 UTC 12 September 2008.

The progression of Typhoon Sinlaku intensity (Fig. 3a) and stages (Fig. 3b) through the ERC is depicted in a Hovmöller diagram of mean positive WVIR BT differences (Fig. 3c) over the 120-h period between 9 and 13 September 2008. Prior to the ERC, eye and eyewall development are evident (Fig. 3c) as regions of near-zero and positive WVIR BT differences, respectively, during the intensification of Sinlaku (Fig. 3a) from tropical storm to typhoon intensity on 9 September 2008. A clear eye and single eyewall (ERC stage 1) became consistently discernable as Sinlaku intensified from 85- to over 100-kt intensity (starting just after 0200 UTC 10 September 2008). Characterized by a region free of deep convection initially to near 10 km, the eye radius increased slightly and remained near 15 km from the TC center for over 24 h. The single eyewall was composed of tropopause-penetrating convection (with WVIR BT differences ranging from 1.5 to 3.5 K) 15–150 km from the TC center.

Around 1700 UTC 10 September 2008, deep convection in the single eyewall began to erode at outer radii, which marked the onset of ERC stage 2 (Fig. 3). Over the next several hours, the average radial extent of the broad eyewall was nearly halved, and deep convection extended radially to only about 75 km from the center by 0000 UTC 11 September 2008. This decrease in the positive WVIR BT differences at outer radii occurred in conjunction with reduced intensification and then slight weakening in the surface wind speeds.

A double eyewall signature was present in the radial profiles at 0600 UTC 11 September 2008, and was indicated in the Hovmöller diagram by two regions of deep convection within 200 km of the TC center, centered at radii of around 30 and 120 km (Fig. 3). The maximum magnitude of positive WVIR differences in both eyewalls was generally lower (between 1.5 and 2.0 K) than in both the previous single eyewall and transition stages (3.0–3.5 K). During this third ERC stage (concentric eyewalls), the TC intensity remained near 120 kt.

The dual maxima in eyewall deep convection was relatively short lived. Decay in the inner eyewall deep convection was evident after about 1300 UTC 11 September 2008, which marked the start of the fourth ERC stage (Fig. 3). This reduction in inner eyewall convection was noted in the 11 September 2008 mission report (Middlebrooke and Sanger 2008) as a weakening of the inner eyewall during the second pass through the TC (center fix time 1331 UTC 11 September 2008). During this fourth ERC stage (decaying inner eyewall), the TC intensity decreased slightly from 120 to 115 kt.

By 0145 UTC 12 September 2008, the eye was free of deep convection previously associated with the inner eyewall, marking the transition to the fifth stage of the ERC (Fig. 3). During this stage, the inner edge of the single eyewall remained nearly 100 km from the TC center until contraction (and the final ERC stage) began at about 1645 UTC 12 September 2008. A gradual increase in the amount of deep convection in the eyewall occurred concurrently with the eyewall contraction. However, instead of increasing in TC intensity (as often occurs during contraction of the outer eyewall), Sinlaku weakened by 10 kt (100 to 90 kt) during the contraction stage as its circulation interacted with the mountainous terrain of Taiwan.

It is important to note that the ERC stages defined here, as well as the transitions between stages, are subjective. Despite this subjectivity, the ERC progression was effectively mapped using the WVIR data, and this visual depiction of the ERC could be beneficial in an operational forecast setting. Analysis of the positive WVIR BT differences is continued in the subsequent section, where plan views and radial profiles are compared to IR BT data during eight reconnaissance aircraft passes through Sinlaku.

b. *Evolution of deep convection during aircraft reconnaissance missions*

The T-PARC–TCS08 field program offered one of the first opportunities to fly through a western North Pacific typhoon since the Office of Naval Research (ONR) Tropical Cyclone Motion field programs in the early 1990s. The four flights through Sinlaku each entailed two transects through the TC center and spanned all phases of the ERC (Fig. 3, Table 1). Examination of the deep convection WVIR BTs and cloud-top temperatures (IR BTs) at the time of each center transect (Fig. 4) coupled with the mean radial profiles of WVIR and IR BTs (Fig. 5) places the flights in the context of the ERC and lays the groundwork for further examination of the wind speeds and BTs along each transect in the subsequent section.

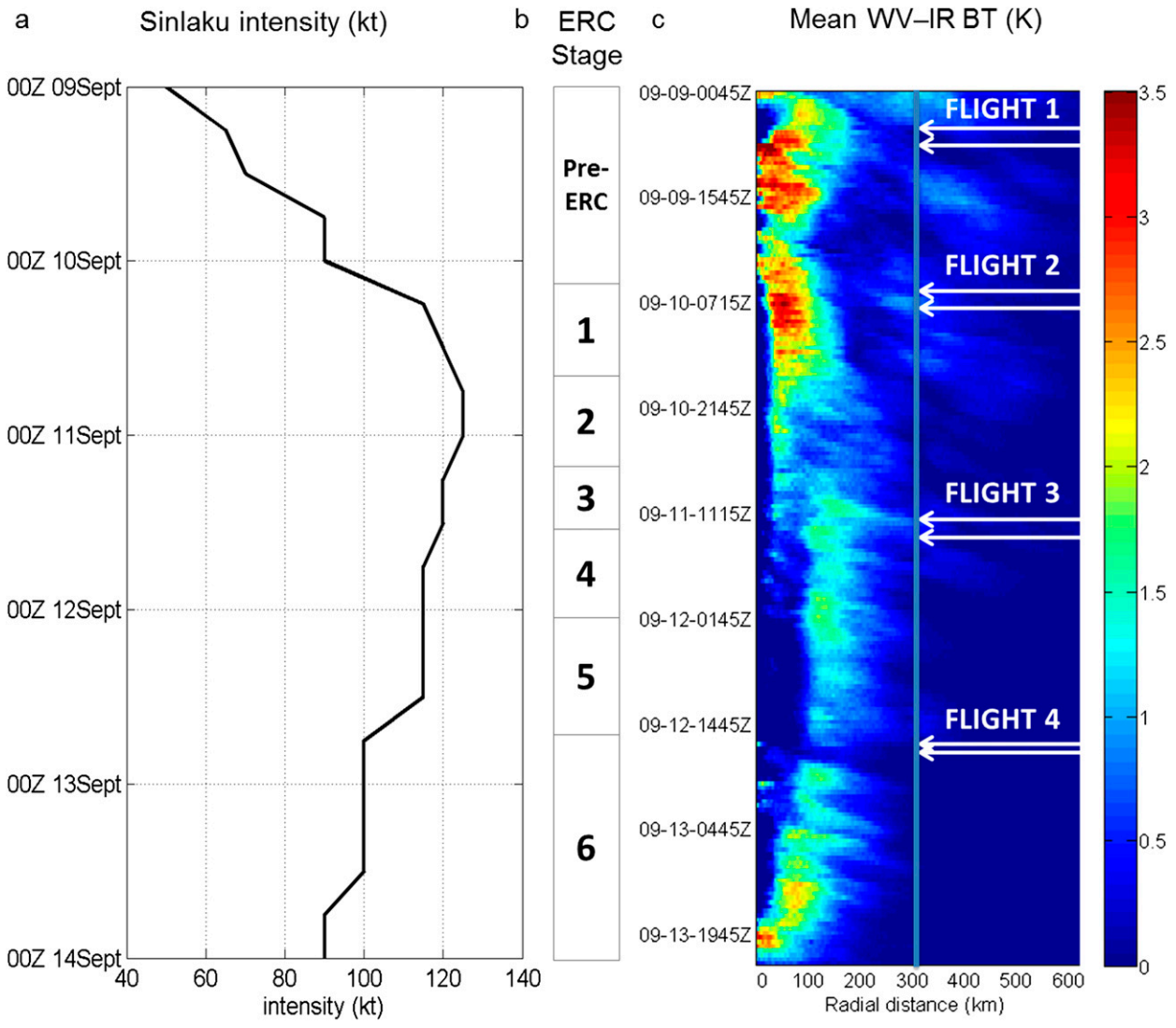

FIG. 3. (a) Intensity (kt), (b) ERC stage, and (c) Hovmöller diagram of azimuthally averaged positive WVIR BT differences (K) for Typhoon Sinlaku. White arrows identify times of the eight aircraft transects, and the blue line at 300-km radius indicates spatial extent in Figs. 4–6. Note that *y*-axis time scales differ slightly due to *MTSAT-1* data availability.

The first flight into Sinlaku, on 9 September 2008, took place during the development of the eye and eyewall prior to the ERC (Fig. 3c). An increase in deep convection surrounding the TC center was evident over the course of the two center transects (Figs. 4a–d). This deep convection development was captured in mean radial profiles of positive WVIR (green curves in Fig. 5) and IR (blue curves in Fig. 5) BT differences. From the center out to 80 km, values of IR BT decreased (cloud tops became colder) and WVIR BTs increased (indicating greater prevalence or magnitude of deep convection) over the 2-h span between 0445 and 0645 UTC 9 September 2008 (Figs. 5a,b). Additionally, deep convection decreased at radii between 100 and 150 km. This change in the distribution of deep convection, particularly near the 40-km radius, corresponded to the development of an eye and primary eyewall. Convective development continued over the subsequent 24 h, and by the 10 September 2008 flight, stage 1 of the ERC (single eyewall) was under way (Fig. 3c). The large single eyewall was noted in both the cold cloud tops (Figs. 4e,f) and deep convection (Figs. 4g,h) data. Positive WVIR BT differences radially inward of about 75 km increased from 0545 to 0745 UTC 10 September 2008 (Figs. 5c,d). Just over 24 h later, on 11 September 2008, a substantial increase in deep convection at outer radii was clearly evident on the southern side of the TC (Figs. 4i–l). Concentric eyewalls were present in both the deep

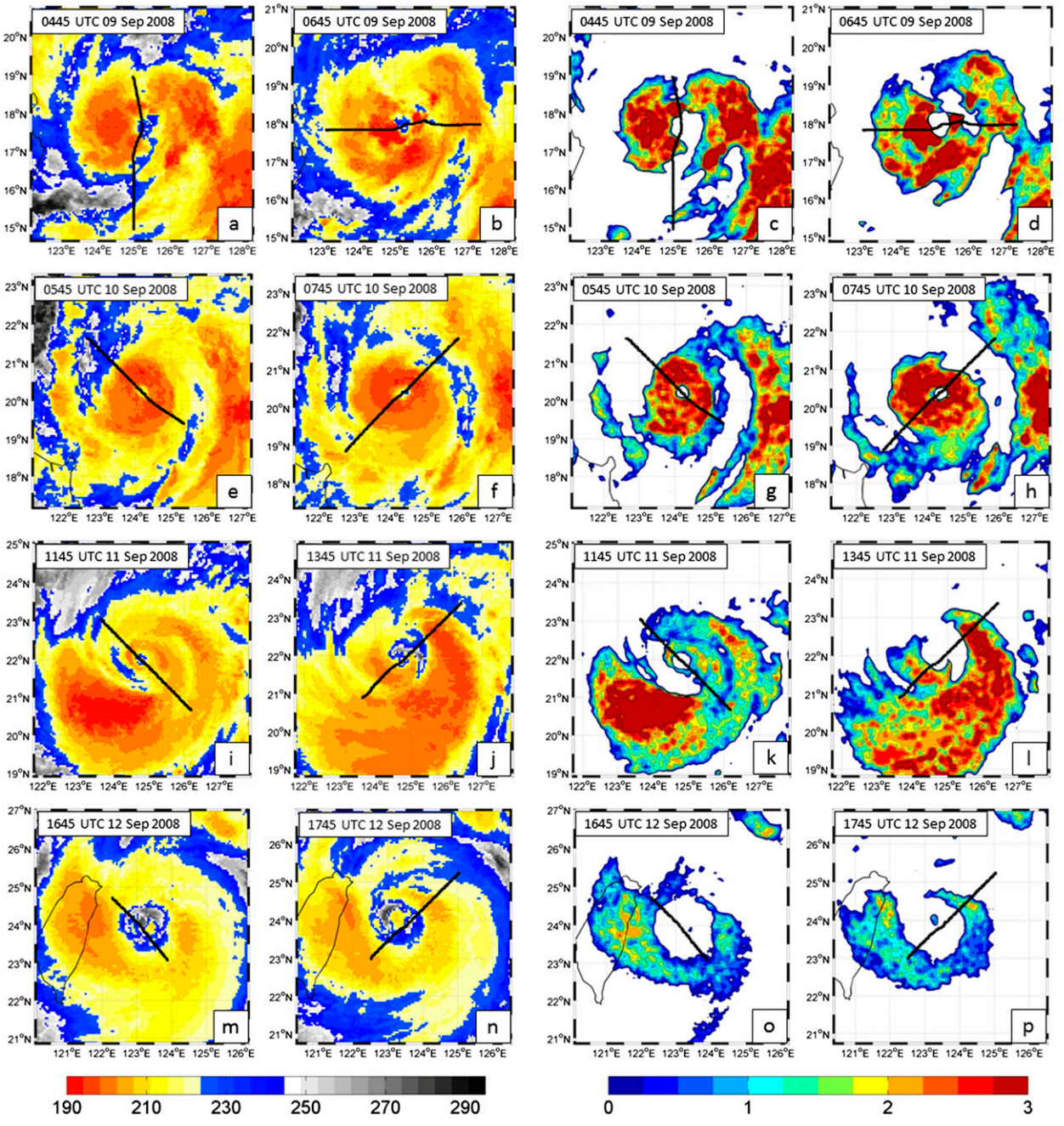

FIG. 4. Infrared (K; columns 1 and 2) and positive WVIR BT differences (K; columns 3 and 4) for the eight flight transects indicated in Fig. 3c. Black lines indicate aircraft track through the TC center. Date and time groupings indicate satellite observation times. Flight start and stop times and corresponding satellite observation times are listed in Table 1.

convection and IR plan views during the first pass through the TC (Figs. 4i,k). The region of deep convection southwest of the center during the southeast–northwest transect rotated cyclonically over the 2 h between center passes, and the inner eyewall also lost coherence during that time, opening to the north (Figs. 4i–l). Mean radial profiles of IR and positive WVIR at 1145 UTC 11 September 2008 (Fig. 5e) indicated concentric eyewalls, with the inner eyewall located about 40 km outward from the storm center and the outer eyewall located about 110 km outward from the storm center. Notably, the outer eyewall was prominent in the WVIR, indicating ERC stage 4 had begun, while dual minima were still present in the IR, indicating Sinlaku was still

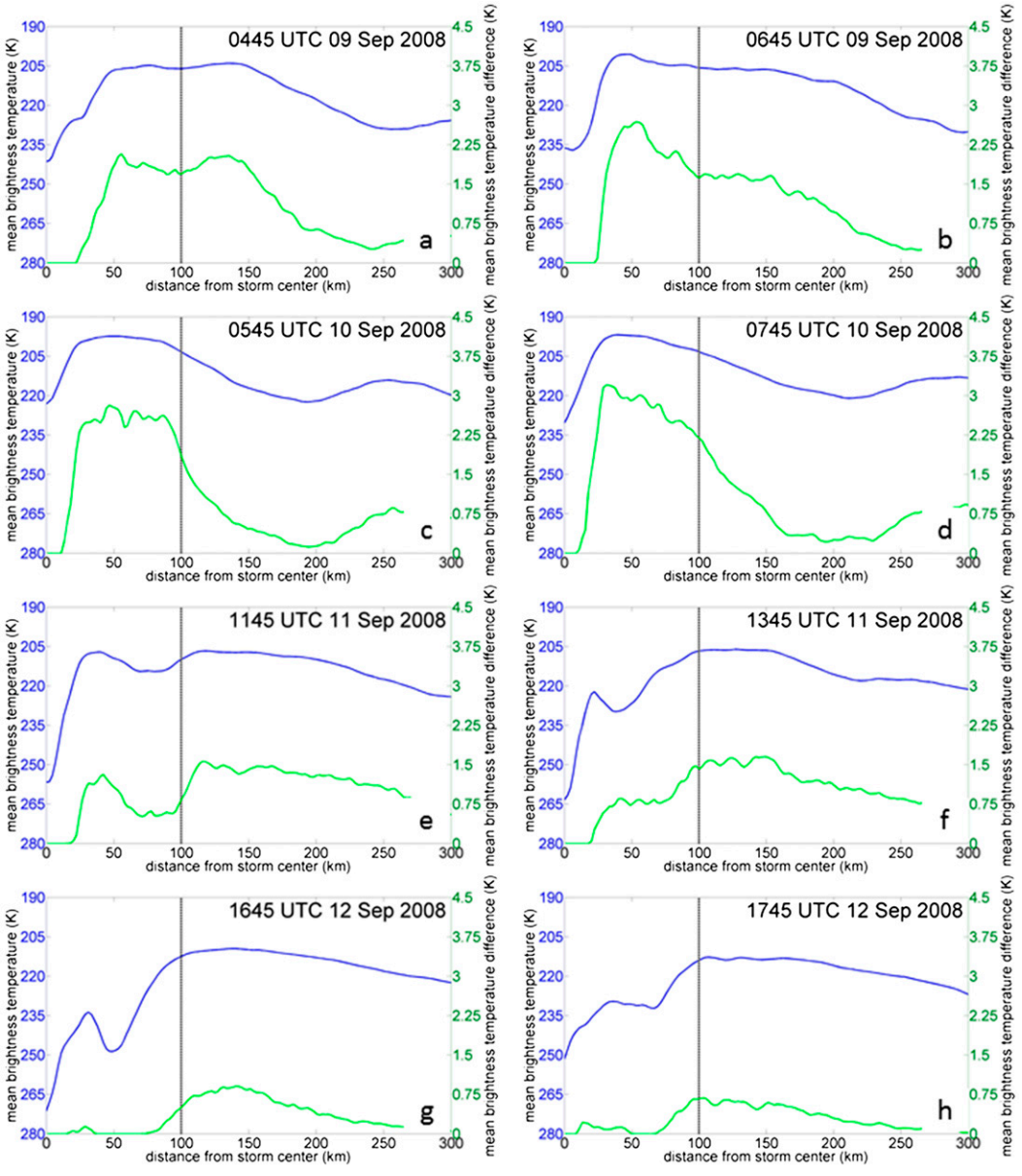

FIG. 5. Mean radial IR (blue) and WVIR (green) BT profiles (K) corresponding to the eight center transects indicated in Fig. 3c and the eight satellite times in Fig. 4. Vertical gray lines mark 100-km radius from the TC center.

in ERC stage 3. Two hours later, during the second transect through the Sinlaku center (Fig. 5f), the prominent (decayed) outer (inner) eyewall associated with ERC stage 4 was clearly evident in the decrease (increase) of the IR BTs and in the increase (decrease) in positive WVIR BTs.

In the 26 h between the final WC-130J center transect on 11 September 2008 and the first on 12 September 2008, Sinlaku continued through stages 4 and 5 of the ERC (Fig. 3). The final two aircraft transects through Sinlaku began at 1627 UTC 12 September 2008 near the start of the contraction phase of the ERC, as the western eyewall made landfall over Taiwan (Figs. 4m–p). Although the TC eye had been free of deep convection for 15 h prior to the arrival of the WC-130J (Fig. 3c), a small area of deep convection was evident in the TC center during both aircraft transects (Figs. 4o,p). At outer radii, deep convection also was weaker than the day prior, particularly north of the TC center. Mean profiles of deep convection highlighted these inner and outer core changes at all radii, indicated by lower positive WVIR BTs (Figs. 5e–h). In contrast, evidence of the inner

eyewall remained in the IR BTs over the 26 h between flights on 11–12 September (not shown) and the remnant cool cloud tops were still present in the inner core during the final two transects (Figs. 4m,n). The mean radial profiles of IR BTs corroborated this, exhibiting dual maxima (on the inverted axes) near 40 and 100 km from the TC center (Figs. 5g,h).

While progression of Sinlaku through the ERC was detected in both IR and WVIR BT profiles, the WVIR mean radial profiles were superior to the IR BT mean profiles in detecting the decay of deep convection in the inner eyewall. Specifically, the WVIR mean profiles led the IR mean profiles (temporally) in the transitions from stage 3 to stage 4 and from stage 4 to stage 5 of the ERC. Analysis of these two satellite products will be continued in the following section, where positive WVIR BT differences and IR BTs corresponding to the actual aircraft track will be examined and compared to surface and flight-level winds measured by the aircraft along the same flight tracks.

c. *Analysis of surface and flight-level wind speeds and satellite BTs during aircraft transects*

The next focus of this study was to examine variability of the surface and flight-level wind speeds and satellite brightness temperatures along the eight flight tracks through the TC center. Fortuitously, 2008 was the first season in which the SFMR instrument was fully integrated as part of the operational equipment configuration onboard the WC-130J (Talbot 2008), enabling measurements of surface winds during hurricane reconnaissance missions. The SFMR surface wind data from 9 September 2008 revealed maximum surface wind speeds below 60 kt (solid red curves, Figs. 6a,b), placing Sinlaku at tropical storm strength. Flight-level winds (dashed red curves, Figs. 6a,b) were similar, although flight-level wind observations were perhaps noisy on the first approach to Sinlaku's storm center (Fig. 6a). Observations from the two flight transects on 10 September 2008 revealed a more intense storm, with maximum surface winds over 80 kt, and maximum flight-level winds near 100 kt, on each transect (Figs. 6c,d). The TC was a mature storm with a developed eye structure and an eyewall with deep convection, and by the second transect, Typhoon Sinlaku was nearing its peak intensity. Dual peaks in SFMR surface winds and flight-level winds were observed during both passes through the TC center. Interestingly, on the inbound segment of pass 1 (Fig. 6c) and the outbound segment of pass 2 (Fig. 6d), secondary maxima in both the surface and flight-level winds were noted around 110 and 120 km, respectively. Given the ERC progression that took place in the subsequent two days, it is likely that these peaks were associated with the development of the secondary wind maximum. Both secondary wind maxima were located on the eastern side of the TC and were radially outward, by about 10 km, of the broad regions of positive WVIR differences that extended radially outward to near 100 km (green curves, Figs. 6c,d). In the IR, a secondary peak was not evident on the southeastern side of the TC center (Fig. 6c), possibly due to the transect length of 150 km. However, a secondary peak was observed 120 km northeast of the center, which was about 10 km radially outward of the secondary wind maximum (on the outbound side of the second transect; blue curve, Fig. 6d).

In the first transect on 11 September 2008 (Fig. 6e), dual maxima (ERC stage 3) were observed in the surface and flight-level winds on both sides of the TC center. On the inbound leg (SE of the TC center), the highest surface and flight-level wind speeds were located in the outer wind maximum, which suggests the decay of the primary eyewall (ERC stage 4) had begun. On the outbound leg (northwest of the TC center; Fig. 6e), however, the strongest surface and flight-level wind speeds were located in the inner wind maximum, indicating the transition to ERC stage 4 had not yet begun northwest of the TC center. Satellite IR BT observations were consistent with the surface wind speed observations during this transect in three ways: first, dual peaks in cold cloud tops were observed on both sides of the TC center; second, the coldest cloud tops were located in the outer (inner) BT minimum on the inbound (outbound) segments; and third, the four coldest cloud tops along the transect were each located radially outward of the surface wind maxima, and less radially outward of the flight-level wind maxima, which is consistent with an outward tilt of the inner core in both eyewalls.

The dual maxima signature in the surface winds was still present during the second center transect on 11 September 2008 (Fig. 6f). An outer surface (flight level) wind maximum was located near 90-km (100-km) radius on both the inbound (southwest) and outbound (northeast) sides of the TC center, and the outer maxima had higher wind speeds than the inner maxima both at the surface and at midlevels. The IR BT profile of the inbound leg showed no sign of an outer peak in close proximity to the outer peak in the SFMR surface wind profile; however, the outbound portion exhibited a very distinct outer peak slightly beyond the outer wind maximum at a radius of nearly 130 km. Positive WVIR differences along the flight track featured a double eyewall structure at 1145 UTC 11 September 2008 and a single eyewall structure at 1345 UTC 11 September 2008, providing additional evidence for the progression of the ERC that was not evident in the IR observations;

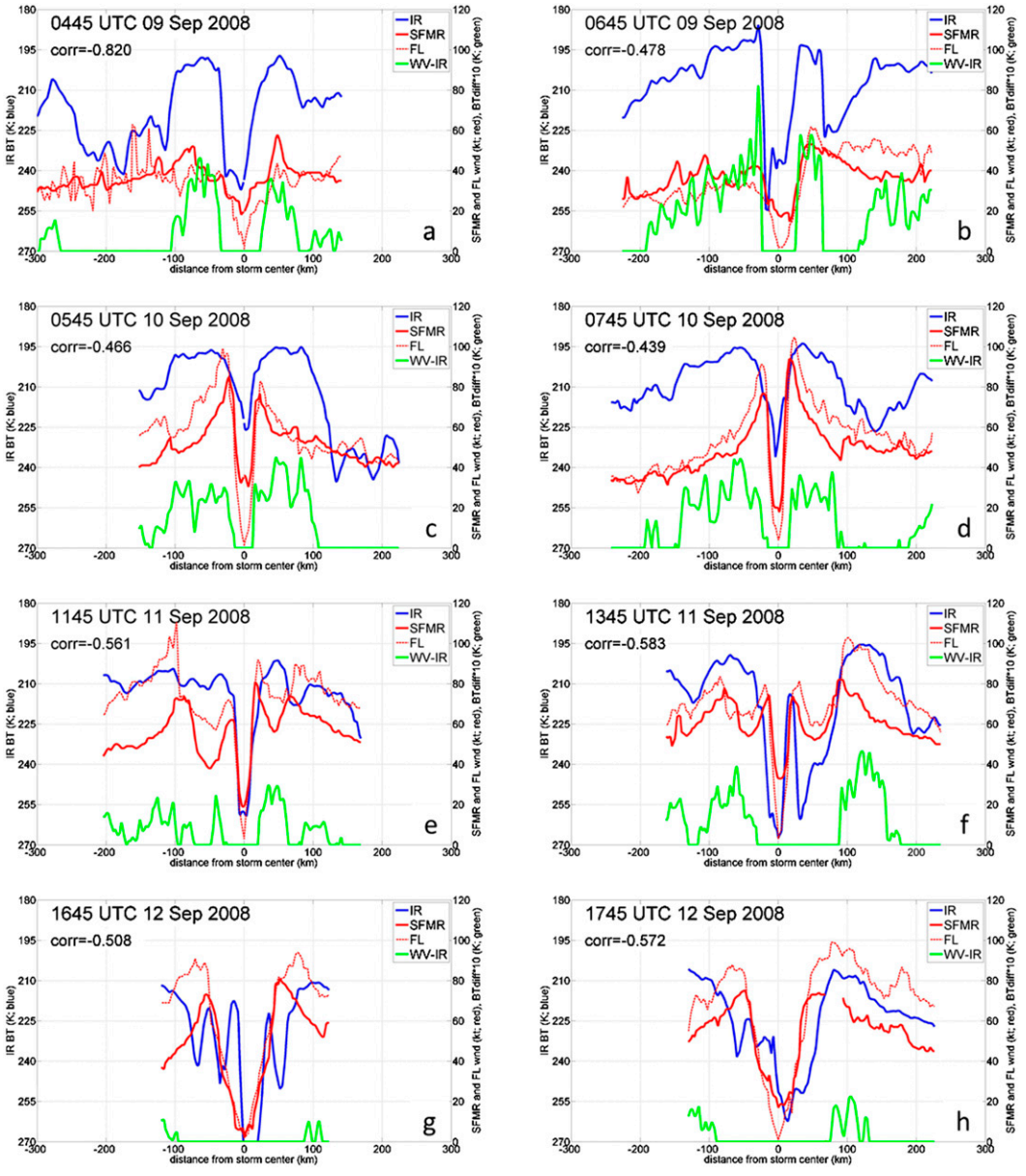

FIG. 6. Infrared BT (K; blue curves), positive WVIR BT differences (K; green curves), SFMR surface winds (kt; solid red curves), and flight-level winds (kt; dashed red curves) along the eight center transects (flight path indicated by black lines in Fig. 4). Correlations between surface wind speed and IR BTs for the inner 100 km (gray line in Fig. 5) are annotated beneath the satellite observation time for each center transect.

however the noisy nature of the WVIR precludes more in-depth analysis.

The temporal lag between the surface wind field and IR BTs was increasingly evident 26 h later. During the first transect on 12 September 2008 (Fig. 6g), a single-peak surface wind speed was present at a radius of near 50 km from the TC center, and a single-peak flight-level wind speed was present at a radius of near 75 km. In the IR observations, however, dual maxima (on the inverted axis) were still present on both sides of the TC center. During the second transect through Sinlaku only a single maximum was present in both IR BTs and SFMR and flight-level winds (Fig. 6h), which indicated that the ERC was complete in the surface and midlevel wind field and in the IR satellite signature. In both flight segments on 12 September 2008, positive WVIR BT differences were small, with maxima around 100 km radially outward from the storm center, indicating that the ERC was complete and that the outer eyewall lacked significant deep convection.

The spatial relationship between surface winds and IR BTs was quantified by Pearson product-moment correlation coefficients. Statistically significant (at the 95% confidence level) negative correlations were present during all transects, ranging from $r = -0.44$ on transect 2 on 10 September 2008 to $r = -0.82$ on transect 1 on 9 September 2008, were found between surface winds and IR BTs. These correlations confirmed that higher surface winds were associated with colder IR BTs, and that this relationship between surface wind and IR BTs held across surface wind intensities ranging from 0 to over 90 kt. Additionally, correlations between SFMR winds and IR BTs were most negative when surface winds spatially lagged IR BTs by 10 km (not shown), with the IR BTs located radially outward of the surface winds. This spatial lag agrees with other work, including that of Sanabia et al. (2014), who found an outward tilt of eyewall convective clouds in IR BT profiles. Because of the noisy nature of the WVIR data along the flight track transects, correlations between WVIR and surface wind were smaller and not generally statistically significant (not shown).

In Sinlaku, maximum surface and flight-level winds were located at radii very near the minimum IR BTs, and this relationship held even through the first three stages of the ERC. This suggests that in an operational setting, profiles of IR BTs could be useful in locating maximum surface winds of a TC. During the final two ERC stages, however, IR BTs were found to temporally lag surface and flight-level winds, indicating that IR BT profiles would not be as useful in identifying radial locations of surface winds in those stages. The WVIR BT differences, while noisy, more closely matched the evolution of the surface wind field during these final two stages, and could be a valuable indicator of radial wind structure late in an ERC.

5. Conclusions

Six ERC stages were defined for the ERC of Typhoon Sinlaku (2008), and the evolution of deep convection through these stages was effectively mapped for the ERC using a Hovmöller diagram. In the Hovmöller diagram, radial changes in positive WVIR BT differences revealed eye and eyewall development and decay. Comparison of these radial changes in deep convection to cloud-top IR BTs at individual time steps revealed that both WVIR and IR BT profiles tracked deep convection during the ERC. However, the decay of deep convection in the inner eyewall (ERC stage 4) was detected first in WVIR mean radial profiles. Comparison of WVIR and IR to wind field measurements along aircraft transects through the TC center yielded two additional results: 1) IR BTs were significantly negatively correlated with surface wind speeds (colder IR temperatures were collocated with stronger surface winds), but they temporally lagged the surface wind speeds at the conclusion of an ERC; and 2) positive WVIR BTs showed the stages of an ERC without any temporal lag, despite not being spatially correlated with the surface wind field. Flight-level wind measurements provided a vertical link between surface wind and cloud-top brightness temperature measurements. Not only did the satellite measurements of cloud-top BTs at the top of the atmosphere agree with the SFMR surface winds (within the boundary layer), they also agreed with the aircraft flight-level winds (within the low to middle troposphere).

Together, these findings highlight the potential utility of WVIR and IR BT radial profiles, particularly so for basins without active aircraft weather reconnaissance programs such as the western North Pacific. Radial profiles of WVIR BT can be useful in detecting CEs and tracking the evolution of a TC through an ERC, including indicating whether single or double wind maxima are present. Profiles of IR BT can be useful in locating the approximate radial positions of surface wind maxima and identifying convective structure before and in the early stages of an ERC (through CE development), but they do not appear to be useful at detecting the concluding stages of an ERC nor in locating radial positions of surface wind maxima during those stages.

Additional work is needed to further examine the utility of WVIR and IR BT profiles, including through Hovmöller-type diagrams, in capturing ERCs during strong TCs. Development of an archive of TC center locations in IR imagery is under way at the Naval Research Laboratory–Monterey (J. Hawkins 2015, personal communication), which will provide a valuable resource for future climatologies using the techniques explored here. Additionally, differences in weighting functions and frequency bands between satellites may impact the utility of these techniques and results. Extending these results beyond a single case study will be important to assessing potential value to forecasters in operational centers.

Acknowledgments. Partial funding for this study was provided by the Office of Naval Research, National Science Foundation, and U.S. Naval Academy Office of Midshipman Research. The authors also gratefully acknowledge the Naval Research Laboratory, Monterey, California, the Japan Meteorological Agency, the Joint Typhoon Warning Center, and the USAF 53rd Weather Reconnaissance Squadron for providing the data on which this research is based.

REFERENCES

Abarca, S. F., and M. T. Montgomery, 2013: Essential dynamics of secondary eyewall formation. *J. Atmos. Sci.,* **70,** 3216–3230, doi:10.1175/JAS-D-12-0318.1.

——, and ——, 2014: Departures from axisymmetric balance dynamics during secondary eyewall formation. *J. Atmos. Sci.,* **71,** 3723–3738, doi:10.1175/JAS-D-14-0018.1.

——, and ——, 2015: Are eyewall replacement cycles governed largely by axisymmetric balance dynamics? *J. Atmos. Sci.,* **72,** 82–87, doi:10.1175/JAS-D-14-0151.1.

Bell, M. M., M. T. Montgomery, and W.-C. Lee, 2012: An axisymmetric view of concentric eyewall evolution in Hurricane Rita (2005). *J. Atmos. Sci.,* **69,** 2414–2432, doi:10.1175/JAS-D-11-0167.1.

Black, M. L., and H. E. Willoughby, 1992: The concentric eyewall cycle of Hurricane Gilbert. *Mon. Wea. Rev.,* **120,** 947–957, doi:10.1175/1520-0493(1992)120<0947:TCECOH>2.0.CO;2.

Chao, C.-C., G.-R. Liu, and C.-C. Liu, 2011: Estimation of the upper-layer rotation and maximum wind speed of tropical cyclones via satellite imagery. *J. Appl. Meteor. Climatol.,* **50,** 750–766, doi:10.1175/2010JAMC2519.1.

Chou, K.-H., C.-C. Wu, P.-H. Lin, S. D. Aberson, M. Weissmann, F. Harnisch, and T. Nakazawa, 2011: The impact of dropwindsonde observations on typhoon track forecasts in DOTSTAR and T-PARC. *Mon. Wea. Rev.,* **139,** 1728–1743, doi:10.1175/2010MWR3582.1.

Cooper, G. A., F. J. Falvey, and M. Vancas, 2009: Annual tropical cyclone report [2008]. U.S. Naval Maritime Forecast Center/Joint Typhoon Warning Center, 116 pp. [Available online at http://www.usno.navy.mil/NOOC/nmfc-ph/RSS/jtwc/atcr/2008atcr.pdf.]

DeMaria, M., 1987: Tropical cyclone track prediction with a barotropic spectral model. *Mon. Wea. Rev.,* **115,** 2346–2357, doi:10.1175/1520-0493(1987)115<2346:TCTPWA>2.0.CO;2.

Elsberry, R. L., and P. A. Harr, 2008: Tropical Cyclone Structure (TCS08) field experiment science basis, observational platforms, and strategy. *Asia-Pac. J. Atmos. Sci.,* **44,** 209–231.

Emanuel, K. A., 2004: Tropical cyclone energetics and structure. *Atmospheric Turbulence and Mesoscale Meteorology,* E. Federovich, R. Rotunno, and B. Stevens, Eds., Cambridge University Press, 165–192.

——, S. Ravela, E. Vivant, and C. Risi, 2006: A statistical-deterministic approach to hurricane risk assessment. *Bull. Amer. Meteor. Soc.,* **87,** 299–314, doi:10.1175/BAMS-87-3-299.

Fritz, S., and I. Laszlo, 1993: Detection of water vapor in the stratosphere over very high clouds in the tropics. *J. Geophys. Res.,* **98,** 22 959–22 967, doi:10.1029/93JD01617.

Hawkins, J. D., and M. Helveston, 2004: Tropical cyclone multiple eyewall characteristics. *26th Conf. on Hurricane and Tropical Meteorology,* Miami, FL, Amer. Meteor. Soc., P1.7. [Available online at https://ams.confex.com/ams/26HURR/techprogram/paper_76084.htm.]

Holland, G., 1980: An analytic model of the wind and pressure profiles in hurricanes. *Mon. Wea. Rev.,* **108,** 1212–1218, doi:10.1175/1520-0493(1980)108<1212:AAMOTW>2.0.CO;2.

——, J. I. Belanger, and A. Fritz, 2010: A revised model for radial profiles of hurricane winds. *Mon. Wea. Rev.,* **138,** 4393–4401, doi:10.1175/2010MWR3317.1.

Houze, R. A., and Coauthors, 2006: The Hurricane Rainband and Intensity Change Experiment (RAINEX): Observations and modeling of Hurricanes Katrina, Ophelia, and Rita (2005). *Bull. Amer. Meteor. Soc.,* **87,** 1503–1521, doi:10.1175/BAMS-87-11-1503.

——, S. S. Chen, B. F. Smull, W.-C. Lee, and M. M. Bell, 2007: Hurricane intensity change and eyewall replacement. *Science,* **315,** 1235–1239, doi:10.1126/science.1135650.

Huang, Y.-H., M. T. Montgomery, and C.-C. Wu, 2012: Concentric eyewall formation in Typhoon Sinlaku (2008). Part II: Axisymmetric dynamical processes. *J. Atmos. Sci.,* **69,** 662–674, doi:10.1175/JAS-D-11-0114.1.

Jaiswal, N., C. M. Kishtawal, and P. K. Pal, 2012: Cyclone intensity estimation using similarity of satellite IR images based on histogram matching approach. *Atmos. Res.,* **118,** 215–221, doi:10.1016/j.atmosres.2012.07.006.

Kaplan, J., and M. DeMaria, 2003: Large-scale characteristics of rapidly intensifying tropical cyclones in the North Atlantic basin. *Wea. Forecasting,* **18,** 1093–1108, doi:10.1175/1520-0434(2003)018<1093:LCORIT>2.0.CO;2.

Kepert, J. D., 2013: How does the boundary layer contribute to eyewall replacement cycles in axisymmetric tropical cyclones? *J. Atmos. Sci.,* **70,** 2808–2830, doi:10.1175/JAS-D-13-046.1.

Knaff, J. A., C. R. Sampson, M. DeMaria, T. P. Marchok, J. M. Gross, and C. J. McAdie, 2007: Statistical tropical cyclone wind radii prediction using climatology and persistence. *Wea. Forecasting*, **22**, 781–791, doi:10.1175/WAF1026.1.

——, ——, P. J. Fitzpatrick, Y. Jin, and C. M. Hill, 2011: Simple diagnosis of tropical cyclone structure via pressure gradients. *Wea. Forecasting,* **26,** 1020–1031, doi:10.1175/WAF-D-11-00013.1.

Kossin, J. P., and M. Sitkowski, 2009: An objective model for identifying secondary eyewall formation in hurricanes. *Mon. Wea. Rev.,* **137,** 876–892, doi:10.1175/2008MWR2701.1.

——, and ——, 2012: Predicting hurricane intensity and structure changes associated with eyewall replacement cycles. *Wea. Forecasting,* **27,** 484–488, doi:10.1175/WAF-D-11-00106.1.

——, J. A. Knaff, H. I. Berger, D. C. Herndon, T. A. Cram, C. S. Velden, R. J. Murnane, and J. D. Hawkins, 2007: Estimating hurricane wind structure in the absence of aircraft reconnaissance. *Wea. Forecasting,* **22,** 89–101, doi:10.1175/WAF985.1.

Kuo, H.-C., C.-P. Chang, Y.-T. Yang, and H.-J. Jiang, 2009: Western North Pacific typhoons with concentric eyewalls. *Mon. Wea. Rev.,* **137,** 3758–3770, doi:10.1175/2009MWR2850.1.

Laing, A., and J. L. Evans, 2010: *Introduction to Tropical Meteorology: A Comprehensive Online and Print Textbook.* 2nd ed., version 2a, COMET Program, University Corporation for Atmospheric Research. [Available online at www.meted.ucar.edu/tropical/textbook_2nd_edition/ (with free registration).]

Lee, C.-S., K. K. W. Cheung, W.-T. Fang, and R. L. Elsberry, 2010: Initial maintenance of tropical cyclone size in the western North Pacific. *Mon. Wea. Rev.,* **138,** 3207–3223, doi:10.1175/2010MWR3023.1.

Leslie, L. M., and G. J. Holland, 1995: On the bogussing of tropical cyclones in numerical models: A comparison of vortex profiles. *Meteor. Atmos. Phys.,* **56,** 101–110, doi:10.1007/BF01022523.

Maclay, K. S., M. DeMaria, and T. H. Vonder Haar, 2008: Tropical cyclone inner-core kinetic energy evolution. *Mon. Wea. Rev.,* **136,** 4882–4898, doi:10.1175/2008MWR2268.1.

Middlebrooke, M., and N. Sanger, 2008: USAF C-130 scientist mission summary report. [Available online at http://catalog.eol.ucar.edu/cgi-bin/tparc_2008/htmlwrap?file_url=/tparc_2008/report/usaf_c130/20080911/report.usaf_c130.200809110728.mission_summary.html.]

Monette, S. A., C. S. Velden, K. S. Griffin, and C. M. Rozoff, 2012: Examining trends in satellite-detected tropical overshooting

tops as a potential predictor of tropical cyclone rapid intensification. *J. Appl. Meteor. Climatol.,* **51,** 1917–1930, doi:10.1175/JAMC-D-11-0230.1.

Olander, T. L., and C. S. Velden, 2009: Tropical cyclone convection and intensity analysis using differenced infrared and water vapor imagery. *Wea. Forecasting,* **24,** 1558–1572, doi:10.1175/2009WAF2222284.1.

Qiu, X., Z.-M. Tan, and Q. Xiao, 2010: The roles of vortex Rossby waves in hurricane secondary eyewall formation. *Mon. Wea. Rev.,* **138,** 2092–2109, doi:10.1175/2010MWR3161.1.

Rozoff, C. M., W. H. Schubert, and J. P. Kossin, 2008: Some dynamical aspects of tropical cyclone concentric eyewalls. *Quart. J. Roy. Meteor. Soc.,* **134,** 583–593, doi:10.1002/qj.237.

Sanabia, E. R., B. S. Barrett, and C. M. Fine, 2014: Relationships between typhoon intensity and eyewall slope as determined by radial profiles of inner-core infrared brightness temperatures. *Mon. Wea. Rev.,* **142,** 4581–4599, doi:10.1175/MWR-D-13-00336.1.

Sitkowski, M., J. P. Kossin, and C. M. Rozoff, 2011: Intensity and structure changes during hurricane eyewall replacement cycles. *Mon. Wea. Rev.,* **139,** 3829–3847, doi:10.1175/MWR-D-11-00034.1.

Talbot, J., 2008: Use of the operational Air Force Reserve Stepped Frequency Microwave Radiometer during the 2007 hurricane season. *62nd Interdepartmental Hurricane Conf.,* Charleston, SC, Office of the Federal Coordinator for Meteorology. [Available online at www.ofcm.noaa.gov/ihc08/linking_file_ihc08.htm.]

Terwey, W. D., and M. T. Montgomery, 2008: Secondary eyewall formation in two idealized, full-physics modeled hurricanes. *J. Geophys. Res.,* **113,** D12112, doi:10.1029/2007JD008897.

Weissmann, M., and Coauthors, 2011: The influence of assimilating dropsonde data on typhoon track and midlatitude forecasts. *Mon. Wea. Rev.,* **139,** 908–920, doi:10.1175/2010MWR3377.1.

Willoughby, H. E., J. A. Clos, and M. G. Shoreibah, 1982: Concentric eye walls, secondary wind maxima, and the evolution of the hurricane vortex. *J. Atmos. Sci.,* **39,** 395–411, doi:10.1175/1520-0469(1982)039<0395:CEWSWM>2.0.CO;2.

——, R. W. R. Darling, and M. E. Rahn, 2006: Parametric representation of the primary hurricane vortex. Part II: A new family of sectionally continuous profiles. *Mon. Wea. Rev.,* **134,** 1102–1120, doi:10.1175/MWR3106.1.

Wimmers, A. J., and C. S. Velden, 2010: Objectively determining the rotational center of tropical cyclones in passive microwave satellite imagery. *J. Appl. Meteor. Climatol.,* **49,** 2013–2034, doi:10.1175/2010JAMC2490.1.

Wood, V. T., L. W. White, H. E. Willoughby, and D. P. Jorgensen, 2013: A new parametric tropical cyclone tangential wind profile model. *Mon. Wea. Rev.,* **141,** 1884–1909, doi:10.1175/MWR-D-12-00115.1.

Wu, C.-C., Y.-H. Huang, and G.-Y. Lien, 2012: Concentric eyewall formation in Typhoon Sinlaku (2008). Part I: Assimilation of T-PARC data based on the ensemble Kalman filter (EnKF). *Mon. Wea. Rev.,* **140,** 506–527, doi:10.1175/MWR-D-11-00057.1.

Yang, Y.-T., H.-C. Kuo, E. A. Hendricks, and M. S. Peng, 2013: Structural and intensity changes of concentric eyewall typhoons in the western North Pacific Basin. *Mon. Wea. Rev.,* **141,** 2632–2648, doi:10.1175/MWR-D-12-00251.1.

Zhou, X., and B. Wang, 2009: From concentric eyewall to annular hurricane: A numerical study with the cloud-resolved WRF model. *Geophys. Res. Lett.*, **36**, L03802, doi:10.1029/2008GL036854.